



Diurnal cycle of land surface temperature in a desert encroachment zone as observed from satellites

R. T. Pinker,¹ D. Sun,² M. Miller,³ and G. J. Robinson⁴

Received 30 March 2007; accepted 8 May 2007; published 9 June 2007.

[1] Climate variability in the African Soudano-Sahel savanna zone has attracted much attention because of the persistence of anomalously low rainfall. Past efforts to monitor the climate of this region have focused on rainfall and vegetation conditions, while land surface temperature (LST) has received less attention. Remote sensing of LST is feasible and possible at global scale. Most remotely sensed estimates of LST are based on the National Oceanic and Atmospheric Administration (NOAA) Advanced Very High Resolution Radiometer (AVHRR) that are limited in their ability to capture the full diurnal cycle. Although more frequent observations are available from past geostationary satellites, their spatial resolution is coarser than that of polar orbiting satellites. In this study, the improved capabilities of the Spinning Enhanced Visible and Infrared Imager (SEVIRI) on the METEOSAT Second Generation (MSG) instrument are used to remotely sense the LST in the African Soudano-Sahel savanna zone at a resolution of 3 km and 15 minutes. In support of the Radiative Atmospheric Divergence using the ARM Mobile Facility (AMF), GERB and AMMA Stations (RADAGAST) project, African Monsoon Multidisciplinary Analyses (AMMA) project and the Department of Energy's Atmospheric Radiation Measurement (ARM) program, the ARM Mobile Facility was deployed during 2006 in this climatically sensitive region, thereby providing a unique opportunity to evaluate remotely sensed algorithms for deriving LST. **Citation:** Pinker, R. T., D. Sun, M. Miller, and G. J. Robinson (2007), Diurnal cycle of land surface temperature in a desert encroachment zone as observed from satellites, *Geophys. Res. Lett.*, *34*, L11809, doi:10.1029/2007GL030186.

1. Introduction

[2] The African sub-Sahel (about 10°–18°N) is frequented by droughts. Climate variability, such as onset and termination dates of the rainy season, desertification, and droughts are major issues of concern [Tarhule and Lamb, 1978]. In response to the 1968–73 drought, research and monitoring has increased and resulted in information on the impacts of droughts [Lamb and Pepler, 1992; Eltahir and Gong, 1996]. Most studies that have monitored surface

conditions in this region are based on the analyses of the Normalized Difference Vegetation Index (NDVI) or on rainfall variability [Buermann *et al.*, 2003; Herrmann *et al.*, 2005]. Due to the close relationship of LST to soil moisture [Sun and Pinker, 2004a], it is an important parameter for monitoring changes in surface conditions, and when combined with the NDVI, has proven invaluable in drought monitoring [Wan *et al.*, 2004]. Interpretation of NDVI in areas of sparse vegetation is still problematic [Huete *et al.*, 1994] and satellite methods for estimating rainfall in arid regions have limitations. Since the sub-Sahel region is predominantly cloud-free, frequent observations of the surface from satellites are possible. Infrared radiometers on polar orbiting satellites have been used successfully to derive LST at 1 km spatial resolution [Becker and Li, 1990; Prata, 1994; Becker and Li, 1995; Coll and Caselles, 1997; Wan and Dozier, 1996; Liang, 2001; Pinheiro *et al.*, 2006]. LST exhibits strong diurnal variation which cannot be captured adequately by a single polar orbiting satellite. Geostationary satellites provide much higher temporal sampling and capture the diurnal cycle of LST over large areas. Sun and Pinker [2003; 2004b] and Sun *et al.* [2006] introduced new split window and triple window algorithms for daytime and nighttime LST retrieval, respectively, using data from the Geostationary Operational Environmental Satellite (GOES-8). These showed promising results, with a root mean square (RMS) error of about 1~2 K. Compared to the GOES 4 km spatial resolution and 30 min temporal resolution, the Spinning Enhanced Visible and Infrared Imager (SEVIRI) on METEOSAT Second Generation (MSG) improves the spatial resolution to 3 km for the visible and infrared channels and temporal resolution to 15 minutes. These features make SEVIRI very attractive for surface temperature retrieval [Sobrino and Romaguera, 2004; Peres and DaCamara, 2005].

[3] The first MSG satellite (Meteosat-8) was launched in August 2002. SEVIRI, the main instrument on MSG, has eight near-infrared and infrared channels centered approximately on 3.9, 6.2, 7.3, 8.7, 9.7, 10.8, 12.0 and 13.4 μm [Schmetz *et al.*, 2002]. The 3.9, 8.7, 10.8, and 12.0 μm channels lie in four atmospheric windows, suitable for the retrieval of LST [Schmid, 2000]. The maximum dynamic range for the 3.9, 10.8 and 12.0 μm channels is 335 K, but only 300 K for the 8.7 μm channel [Mueller *et al.*, 1999; Pili, 2000], which may limit the latter's use for retrieving land-surface properties [Garrat, 1992].

[4] In this study, we use new three and four channel SEVIRI algorithms for surface temperature (ST) retrievals (also applicable for sea surface temperature), which use observations in the 10–12 μm split window (10.8, 12.0 μm channels), two NIR channels (3.9 and 8.7 μm) [Sun and Pinker, 2007]. The NIR 3.9 μm channel has low atmo-

¹Department of Atmospheric and Oceanic Science, University of Maryland at College Park, College Park, Maryland, USA.

²Center for Earth Observing and Space Research, George Mason University, Fairfax, Virginia, USA.

³Environmental Sciences Department, Brookhaven National Laboratory, Upton, New York, USA.

⁴Environmental Systems Science Centre, University of Reading, Reading, UK.

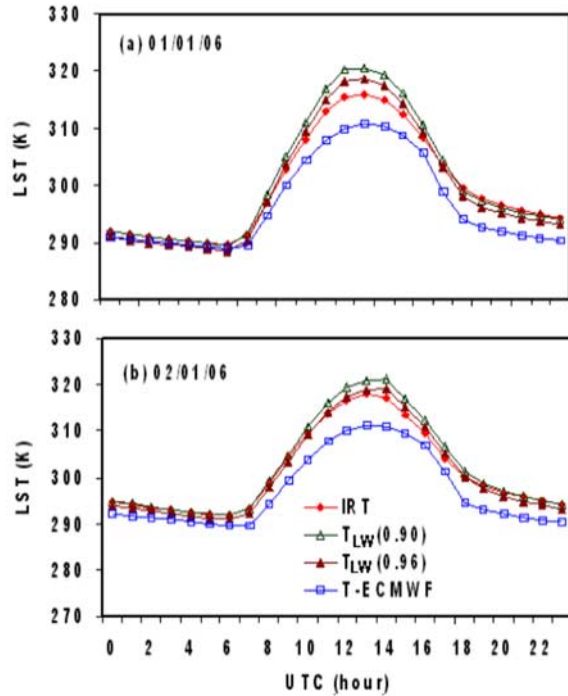


Figure 1. LST at the ARM Niamey, Niger, West Africa (N 13° 28.638', E 2° 10.547') site as obtained from ARM measured infrared temperature (IRT), from long-wave radiation (LW) by assuming surface emissivity as 0.90 ($T_{LW}(0.90)$) and 0.96 ($T_{LW}(0.96)$), and from the ECMWF reanalysis (T-ECMWF).

spheric absorption and attenuation [May and Holyer, 1993; Sun and Pinker, 2003], which can be used to improve atmospheric correction. However, it contains a contribution from solar radiation during daytime, and this must be accounted for. Section 2 describes the data used in this study. Section 3 presents the methodology used, which is based on linearization of the radiative transfer equation, and aims to improve atmospheric correction by using the characteristics of the NIR channel. Section 5 presents results from the new algorithms, compared with those from other published studies that use a popular generalized split-window algorithm [Becker and Li, 1990; Wan and Dozier, 1996].

2. Data

2.1. Background

[5] An opportunity to evaluate the new SEVIRI LST algorithms [Sun and Pinker, 2007] in a desert encroachment zone arose from the independent deployment of the Atmospheric Radiation Measurement (ARM) Program mobile facility (AMF) in Africa in response to a proposal entitled 'Radiative Atmospheric Divergence using the ARM Mobile Facility (AMF), GERB and AMMA STations' (RADAGAST) [Miller and Slingo, 2007]. The objective of RADAGAST was to combine an extended series of measurements from the AMF with those from SEVIRI and the Geostationary Earth Radiation Budget (GERB) broad-band Earth radiation budget instrument, also on MSG, to provide the first well-sampled, direct estimates of the divergence of solar and thermal radiation across the atmosphere. The location of the AMF site was chosen partly to take advan-

tage of the logistic infrastructure of the simultaneous field campaign phase and Special Observing Periods (SOP) of AMMA, an international project that is concerned with the broader climatic impacts of the West African Monsoon at both local and regional scales (<http://www.amma-international.org/>). This location also presents a unique challenge to radiative transfer models, because of the high variation in total atmospheric water column, episodic mineral dust events [Slingo *et al.*, 2006] and seasonal aerosols from biomass burning. The main site is located near the Airport (N13° 28.638', E2° 10.547', 205 m), with an ancillary site at Banizoumbou (N 13° 31.319', E 2° 37.941').

2.2. Ground and Satellite Data

[6] Surface observations at Niamey and subsets of ECMWF analyses used in this study were obtained from the ARM data archive: <http://www.archive.arm.gov>.

[7] Time series of SEVIRI brightness temperature data from the Niamey site were obtained from the RADAGAST web site: http://radagast.nerc-essc.ac.uk/MSG/SEVIRI/TIME_SERIES/. The thermal IR channels of SEVIRI are calibrated by EUMETSAT using an onboard blackbody to accuracy better than 0.5 K [Pili, 2000]. The conversion from radiances to equivalent brightness temperature was performed within the RADAGAST processing system using an analytic relationship, based on the spectral Planck function, provided by EUMETSAT. Geo-location, solar zenith angles, and satellite zenith angles were calculated using routines in the SEVIRI Pre-Processing Toolbox [Govaerts *et al.*, 2005].

2.3. Emissivity

[8] Emissivity is a dynamic parameter that changes with surface conditions such as soil moisture and vegetation state. Satellite methods for its determination are ideal, but as yet they are not fully validated. Therefore, users tend to rely on libraries of emissivity that are compiled for global scale use. Ogawa *et al.* [2003] have estimated broadband emissivity from narrowband emissivities of the five thermal infrared channels of the Advanced Space-borne Thermal Emission and Reflection Radiometer (ASTER). Using a multiple-regression based on data acquired in 2001 and 2002 over a 240 x 1200 km desert area in North Africa, they found significant differences ranging from -0.08 to + 0.06 when compared to a classification-based emissivity map, thus affecting the retrieved temperatures.

3. Methodology

[9] As described by Sun and Pinker [2007], the following SEVIRI LST algorithms have been developed and are used in this study:

[10] Four-channel (4ch) algorithm

$$\begin{aligned} \text{Daytime : } LST(l) = & a_0(l) + a_1(l)T_{10.8} + a_2(l)(T_{10.8} - T_{12.0}) \\ & + a_3(l)(T_{3.9} - T_{8.7}) + a_4(l)(T_{10.8} - T_{12.0})^2 \\ & + a_5(l)(\sec \theta - 1) + a_6(l)T_{3.9} \cos \theta_s \quad (1a) \end{aligned}$$

$$\begin{aligned} \text{Nighttime : } LST(l) = & b_0(l) + b_1(l)T_{10.8} + b_2(l)(T_{10.8} - T_{12.0}) \\ & + b_3(l)(T_{3.9} - T_{8.7}) + b_4(l)(T_{10.8} - T_{12.0})^2 \\ & + b_5(l)(\sec \theta - 1) \quad (1b) \end{aligned}$$

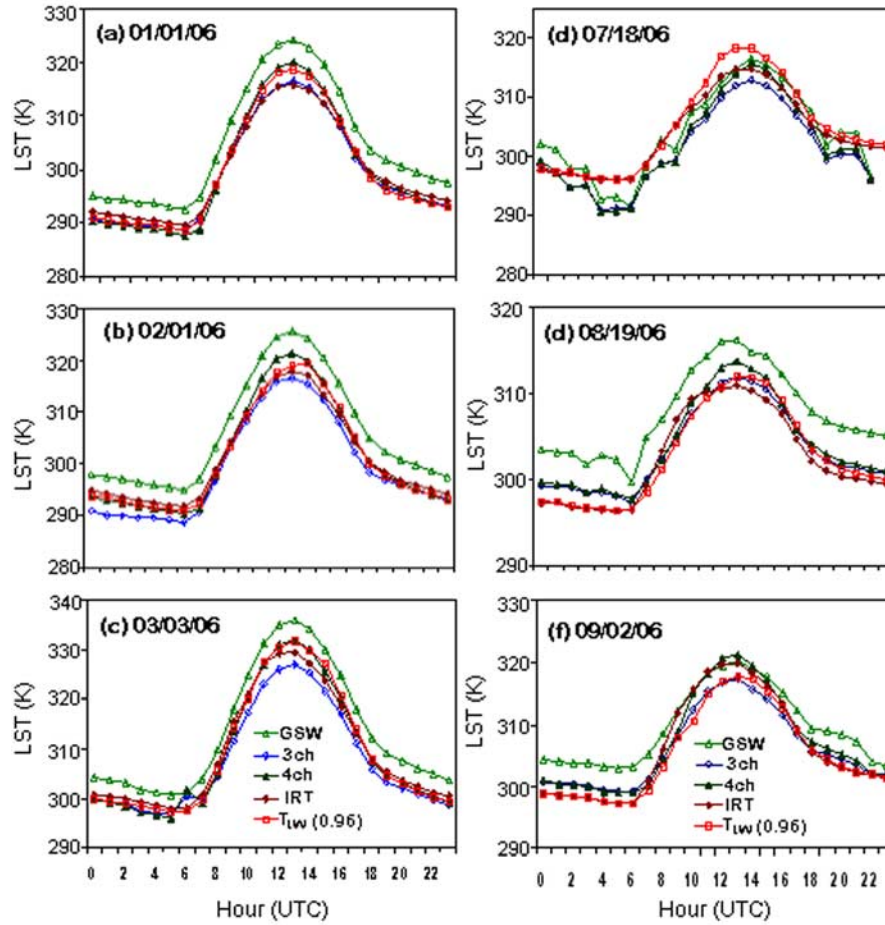


Figure 2. LST retrieval from the MSG/SEVIRI measurements using the generalized split window (GSW); the proposed three-channel (3ch) SEVIRI algorithm; the new proposed SEVIRI four-channel (4ch) algorithms; and ground skin temperature as derived from the infrared observations (IRT) and converted from upwelling observations with assumed surface emissivity of 0.96 ($T_{LW}(0.96)$), for the following days: (a) 01/01/06, (b) 02/01/06, (c) 03/03/06, (d) 07/18/06, (e) 08/19/06, and (f) 09/02/06.

where l is the surface type index, T is equivalent brightness temperature, θ is the viewing angle, θ_s is the solar zenith angle, and the subscripts refers to the SEVIRI IR channels. In the implementation of the above algorithms, the coefficients are determined according to surface type (desert in this case).

4. Comparison With Emissivity Approach

[11] Three-channel (3ch) algorithm for daytime and nighttime:

$$LST = a_0 + a_1 T_{10.8} + a_2 T_{12.0} + a_3 T_{8.7} + a_4 \frac{(1 - \varepsilon_{10.8})}{\varepsilon_{10.8}} T_{10.8} + a_5 \frac{(1 - \varepsilon_{12.0})}{\varepsilon_{12.0}} T_{12.0} + a_6 \frac{(1 - \varepsilon_{8.7})}{\varepsilon_{8.7}} T_{8.7} + a_7 (\sec \theta - 1) \quad (2)$$

[12] The spectral channel emissivity in this algorithm can be derived according to the methodology of *Peres and DaCamara* [2005].

[13] Generalized split-window [*Becker and Li, 1990; Wan and Dozier, 1996*]

$$LST = P \frac{T_{10.8} + T_{12.0}}{2} + M(T_{10.8} - T_{12.0}) + C \quad (3)$$

[14] *Wan and Dozier* [1996] optimized the above local split-window algorithm [*Becker and Li, 1990*] to a generalized split-window (GSW) algorithm, by computing coefficients that vary with satellite zenith angle (SZA), water vapor, and lower boundary air temperature.

5. Evaluation at Niamey, Niger

[15] Surface temperature can be derived from ground observations of long-wave (LW) upwelling and downwelling radiation [*Zhou et al., 2003*]:

$$T_{LW} = [(LW^\uparrow - (1 - \varepsilon)LW^\downarrow)/(\varepsilon\sigma)]^{1/4} \quad (4)$$

or from infrared thermometer (IRT) measurements. In this study equation (4) is applied to LW observations at the AMF site, where ε is the surface broadband emissivity and σ is the Stefan-Boltzman constant. The emissivity was assumed to be $\varepsilon = 0.90$ (as given in the Spectral Library of JPL) and 0.96 (as derived by *Ogawa et al.* [2003]). The values of IRT reported at the AMF web site are estimated from the Stefan-

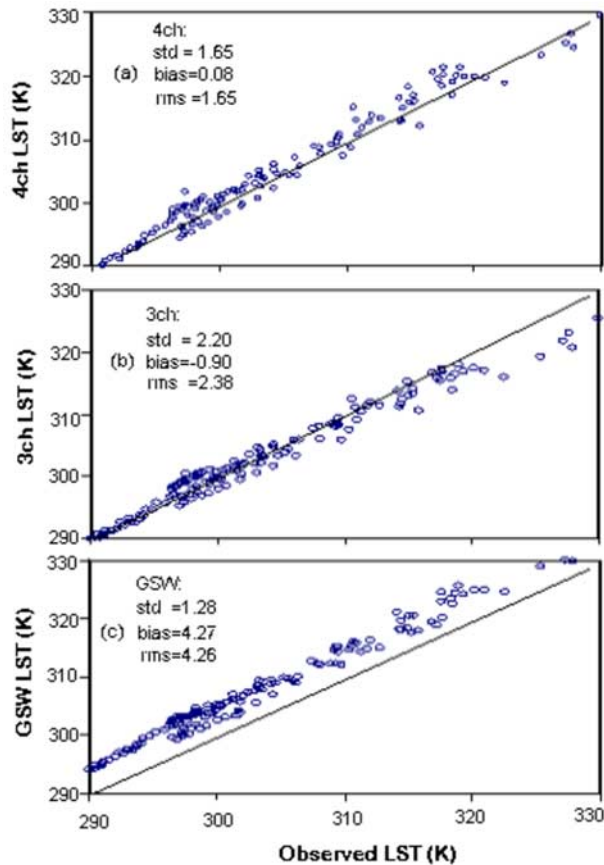


Figure 3. LST retrieval (std, bias, and rms) errors from different algorithms: (a) four-channel (4ch), (b) three-channel (3ch), and (c) generalized split window (GSW).

Boltzman Law assuming $\varepsilon = 1$ [Steffel, 2004a; Steffel, 2004b; Morris, 2006].

6. Results

[16] The effect of the assumed emissivity on estimates of the “ground reference” LST at the AMF site over two clear sky days is illustrated in Figure 1. This shows that an emissivity increase from 0.90 to 0.96 can reduce LST by 1–2 K; an emissivity change from 0.90 to 1.0 (IRT) can reduce LST by as much as 1.5–3.5 K. The model-derived skin temperature from the ECMWF (European Centre for Medium-Range Weather Forecasts) obtained from the ARM archive is shown for comparison. Figure 1 shows that modeled skin temperature can be about 5–6 K lower than IRT at the hottest time of the day. As discussed by Fuchs [1990] and Fiebrich *et al.* [2003], the assumption of unity surface emissivity in the estimation of IRT leads to underestimation of skin temperature because surface emissivity can be less than 1.0, while neglecting surface reflection of downwelling long-wave radiation causes overestimation. If T_{LW} (0.96) is corrected for the reflected radiation, comparison with the IRT shows the integral effect is an underestimate, especially during daytime (–0.73 K on the average).

[17] The algorithms (equations 1–3) were applied to the SEVIRI observations at the AMF Niamey site. Potentially clear days were selected using the daily log of meteorological conditions provided on the RADAGAST web site

(<http://radagast.nerc-essc.ac.uk>). To identify completely clear days a simple cloud mask was then applied using the brightness temperature difference between 11 and $3.9 \mu\text{m}$, according to: $T_{11}-T_{3.9} > -10 \text{ K}$, as a filter. The spectral surface emissivity at 10.8 and $12.0 \mu\text{m}$ required for the generalized split window (GSW) and three-channel (3ch) algorithms at the Niamey site were estimated from the MSG data according to the method proposed by Peres and DaCamara [2005].

[18] LST retrievals from the SEVIRI measurements were generated using the GSW algorithm and the new 3ch and 4ch SEVIRI algorithms. The ground observed LST was converted from the long-wave observations with assumed surface emissivity of 0.96 T_{LW} (0.96). Figure 2 shows these results for the following days: 01/01/06 (Figure 2a), 02/01/06 (Figure 2b), 03/03/06 (Figure 2c), 07/18/06 (Figure 2d), 08/19/06 (Figure 2e), and 09/02/06 (Figure 2f).

[19] Figure 3 and Table 1 provide a statistical summary of the cases presented in Figure 2. As evident, the four-channel algorithm yields the smallest bias.

[20] Figure 2 indicates that during winter and spring the estimates of LST from the three-channel algorithm ($8.7 \mu\text{m}$, 10.8 and $12.0 \mu\text{m}$) are close to T_{IRT} but during summer and fall they are lower. These estimates are lower than T_{LW} (0.96) for all seasons, possibly, due to the restricted dynamic range of the $8.7 \mu\text{m}$ channel (only up to 300 K). Sun and Pinker [2007] found that if the brightness temperature (T_b) of the $8.7 \mu\text{m}$ channel is below 300 K, the three-channel algorithm is useful. Over the Niamey site, the brightness temperature in the $8.7 \mu\text{m}$ channel is usually above 300 K. The four-channel algorithm does not include the $8.7 \mu\text{m}$ channel directly, only the brightness temperature difference between the 3.9 and $8.7 \mu\text{m}$ channels ($T_{3.9}-T_{8.7}$). Since the coefficient of this difference term for the desert environment is small the effect of the $8.7 \mu\text{m}$ channel may not be as significant as in the three-channel algorithm, and therefore the four-channel algorithm shows improvement over the GSW algorithm which gives an overestimate of 4 K on the average.

7. Conclusions and Discussions

[21] Two algorithms have been implemented with SEVIRI observations and compared with independently developed algorithms (as modified for application with SEVIRI) and with ground observations of LST. The feasibility to estimate LST from SEVIRI at improved accuracies in respect to other available methods has been demonstrated. LST is an important parameter that can be used to detect desertification in

Table 1. Comparison of LST Retrieval Errors From Different Algorithms

| | 4ch | 3ch | GSW |
|-----------------------------------|------|-------|------|
| Residual standard deviation (std) | | | |
| Night | 1.47 | 1.34 | 1.22 |
| Day | 1.85 | 2.60 | 1.45 |
| Bias | | | |
| Night | 0.09 | –0.07 | 4.25 |
| Day | 0.07 | –1.89 | 4.29 |
| RMS | | | |
| Night | 1.47 | 1.35 | 4.43 |
| Day | 1.86 | 3.22 | 4.53 |

areas prone to droughts. Since the methodology used for estimating LST is applicable both during daytime and nighttime, it is possible to derive the Diurnal Temperature Range (DTR), a climate change index that can be directly linked to soil moisture [Braganza et al., 2004]. It is planned to expand this work in such a direction and evaluate the usefulness of the DTR against other available indices of surface conditions (i.e., various vegetation indices).

[22] **Acknowledgments.** The first two authors were supported by NASA grant NNG05GB35G under the Coordinated Enhanced Observing Period (CEOP) activity. We thank Y. Govaert for providing information on the calibration of SEVIRI.

References

- Becker, F., and Z. L. Li (1990), Toward a local split window method over land surface, *Int. J. Remote Sens.*, *11*, 369–393.
- Becker, F., and Z. L. Li (1995), Surface temperature and emissivity at various scales: Definition, measurement and related problems, *Remote Sens. Rev.*, *12*, 225–253.
- Braganza, K., D. J. Karoly, and J. M. Arblaster (2004), Diurnal temperature range as an index of global climate change during the twentieth century, *Geophys. Res. Lett.*, *31*, L13217, doi:10.1029/2004GL019998.
- Buermann, W., B. Anderson, C. J. Tucker, R. E. Dickinson, W. Lucht, C. S. Potter, and R. B. Myneni (2003), Interannual covariability in Northern Hemisphere air temperatures and greenness associated with El Niño–Southern Oscillation and the Arctic Oscillation, *J. Geophys. Res.*, *108*(D13), 4396, doi:10.1029/2002JD002630.
- Coll, C., and V. Caselles (1997), A split-window algorithm for land surface temperature from Advanced Very High-Resolution Radiometer data: Validation and algorithm comparison, *J. Geophys. Res.*, *102*, 16,697–16,713.
- Eltahir, E. A. B., and C. L. Gong (1996), Dynamics of wet and dry years in West Africa, *J. Clim.*, *9*(5), 1030–1042.
- Fiebrich, C. A., J. E. Martinez, J. A. Brotzge, and J. B. Basara (2003), The Oklahoma Mesonet's skin temperature network, *J. Atmos. Oceanic Technol.*, *20*, 1496–1504.
- Fuchs, M. (1990), Canopy thermal infrared observations, *Remote Sens. Rev.*, *5*, 323–333.
- Garrat, J. R. (1992), Extreme maximum land surface temperature, *J. Appl. Meteorol.*, *31*(9), 1096–1105.
- Govaerts, Y., S. Wagner, and M. Clerici (2005), SEVIRI native format pre-processing toolbox user's guide version 2.2, *Rep. EUM/OPS-MSG/TEN/03/0011*, EUMETSAT, Darmstadt, Germany.
- Herrmann, S. M., A. Anyamba, and C. J. Tucker (2005), Recent trends in vegetation dynamics in the African Sahel and their relationship to climate, *Global Environ. Change*, *15*(4), 394–404.
- Huete, A., C. Justice, and H. Liu (1994), Development of vegetation and soil indexes for MODIS-EOS, *Remote Sens. Environ.*, *49*, 224–234.
- Lamb, P. J., and R. A. Peppler (1992), Further case studies of tropical Atlantic surface atmospheric and oceanic patterns associated with sub-Saharan drought, *J. Clim.*, *5*(5), 476–488.
- Liang, S. (2001), An optimization algorithm for separating land surface temperature and emissivity from multi-spectral thermal infrared imagery, *IEEE Trans. Geosci. Remote Sens.*, *39*, 264–274.
- May, D. A., and R. J. Holyer (1993), Sensitivity of satellite multi-channel sea-surface temperature retrievals to the air-sea temperature difference, *J. Geophys. Res.*, *98*, 12,567–12,577.
- Miller, M. A., and A. Slingo (2007), The Atmospheric Radiation Measurement (ARM) Mobile Facility (AMF) and its first international deployment: Measuring radiative flux divergence in West Africa, *Bull. Am. Meteorol. Soc.*, in press.
- Morris, V. R. (2006), Infrared thermometer handbook, *Rep. ARM TR-015*, U.S. Dep. of Energy, Washington, D. C.
- Mueller, J., et al. (1999), Gerb: An Earth radiation budget instrument on second generation Meteosat, *Adv. Space Res.*, *24*(7), 921–924.
- Ogawa, K., T. Schmugge, F. Jacob, and A. French (2003), Estimation of land surface window (8–12 μm) emissivity from multi-spectral thermal infrared remote sensing—A case study in a part of Sahara Desert, *Geophys. Res. Lett.*, *30*(2), 1067, doi:10.1029/2002GL016354.
- Peres, L. F., and C. C. DaCamara (2005), Emissivity maps to retrieve land-surface temperature from MSG/SEVIRI, *IEEE Trans. Geosci. Remote Sens.*, *43*, 1834–1844.
- Pili, P. (2000), Calibration of SEVIRI, paper presented at 2000 EUMETSAT Meteorological Satellite Data Users' Conference, EUMETSAT, Bologna, Italy, 29 May–2 June.
- Pinheiro, A. C. T., R. Mahoney, J. L. Privette, and J. C. Tucker (2006), Development of a daily long term record of NOAA-14 AVHRR land surface temperature over Africa, *Remote Sens. Environ.*, *103*, 153–164.
- Prata, A. J. (1994), Land surface temperature derived from the Advanced Very High Resolution Radiometer and the Along-Track Scanning Radiometer: 2. Experimental results and validation of AVHRR algorithms, *J. Geophys. Res.*, *99*, 13,025–13,058.
- Schmetz, J., P. Pili, S. Tjemkes, D. Just, J. Kerkmann, S. Rota, and A. Ratier (2002), An introduction to Meteosat Second Generation (MSG), *Bull. Am. Meteorol. Soc.*, *83*, 977–992.
- Schmid, J. (2000), The SEVIRI instrument, paper presented at 2000 EUMETSAT Meteorological Satellite Data Users' Conference, EUMETSAT, Bologna, Italy, 29 May–2 June.
- Slingo, A., et al. (2006), Observations of the impact of a major Saharan dust storm on the atmospheric radiation balance, *Geophys. Res. Lett.*, *33*, L24817, doi:10.1029/2006GL027869.
- Sobrino, J. A., and M. Romaguera (2004), Land surface temperature retrieval from MSG1-SEVIRI data, *Remote Sens. Environ.*, *92*, 247–254.
- Steffel, T. (2004a), SKYRAD handbook, *Rep. ARM TR-026*, U.S. Dep. of Energy, Washington, D. C.
- Steffel, T. (2004b), GNDRAD handbook, *Rep. ARM TR-027*, U.S. Dep. of Energy, Washington, D. C.
- Sun, D., and R. T. Pinker (2003), Estimation of land surface temperature from a Geostationary Operational Environmental Satellite (GOES-8), *J. Geophys. Res.*, *108*(D11), 4326, doi:10.1029/2002JD002422.
- Sun, D., and R. T. Pinker (2004a), Case study of soil moisture effect on land surface temperature retrieval, *IEEE Trans. Geosci. Remote Sens. Lett.*, *1*(2), 127–130.
- Sun, D., and R. T. Pinker (2004b), Land surface temperature estimation from the next generation Geostationary Operational Environmental Satellite GOES M-Q, *J. Appl. Meteorol.*, *43*, 363–372.
- Sun, D., and R. T. Pinker (2007), Surface temperature retrieval from MSG-SEVIRI observations, *Int. J. Remote Sens.*, in press.
- Sun, D., R. T. Pinker, and M. Kafatos (2006), Diurnal temperature range over the United States: A satellite view, *Geophys. Res. Lett.*, *33*, L05705, doi:10.1029/2005GL024780.
- Tarhule, A., and P. J. Lamb (1978), Large-scale tropical Atlantic surface circulation patterns associated with sub-Saharan weather anomalies, *Tellus*, *30*, 240–251.
- Wan, Z., and J. Dozier (1996), A generalized split-window algorithm for retrieving land-surface temperature from space, *IEEE Trans. Geosci. Remote Sens.*, *34*, 892–905.
- Wan, Z., P. Wang, and X. Li (2004), Using MODIS Land Surface Temperature and Normalized Difference Vegetation Index products for monitoring drought in the southern Great Plains, USA, *Int. J. Remote Sens.*, *25*, 61–72.
- Zhou, L., R. E. Dickinson, Y. Tian, M. Jin, K. Ogawa, H. Yu, and T. Schmugge (2003), A sensitivity study of climate and energy balance simulations with use of satellite-derived emissivity data over the northern Africa and the Arabian peninsula, *J. Geophys. Res.*, *108*(D24), 4795, doi:10.1029/2003JD004083.

M. Miller, Environmental Sciences Department, Brookhaven National Laboratory, Building 490D, Upton, NY 11973, USA.

R. T. Pinker, Department of Atmospheric and Oceanic Science, University of Maryland at College Park, Space Science Building, College Park, MD 20742-2425, USA. (pinker@atmos.umd.edu)

G. J. Robinson, Environmental Systems Science Centre, University of Reading, Harry Pitt Building, Whiteknights, Reading RG6 6AL, UK.

D. Sun, Center for Earth Observing and Space Research, George Mason University, 1014D David King Hall, 4400 University Drive, Fairfax, VA 22030, USA.